Collapse and Earthquake Swarm after North Korea's 3 September 2017 Nuclear Test

AGU 2017
S43H-2968

Dongdong Tian[1] (dongzhi@mail.ustc.edu.cn), Jiayuan Yao[1], Lianxing Wen[2,1]

1. Laboratory of Seismology and Physics of Earth's Interior; School of Earth and Space Sciences, University of Science and Technology of China
2. Department of Geosciences, Stony Brook University

1. Introduction

On 3 September 2017, the Democratic People's Republic of Korea (North Korea) announced that it had successfully conducted a thermonuclear test. The nuclear test was collaborated by reports of a seismic event with a magnitude ranging from 6.1 to 6.3 by many governmental and international agencies. Unlike the previous nuclear tests in the region, this nuclear test was followed by a series of small seismic events, with the first one occurring about eight-and-a-half minutes after the nuclear test, two on 23 September 2017, and one on 12 October 2017. While the characteristics of these seismic events would carry crucial information about current geological state and environmental condition of the nuclear test site, the precise locations and nature of these seismic events are unknown. In this study, we present high-precision determination of their relative locations and detailed source information about those events and discuss their implications to the status of the nuclear test site and environmental and geological impacts in the region.

Table 1. Locations and origin times of events in this study.

Event ID	Date	Time	Latitude (°N)	Longitude (°E)	Depth (km)	Note
20170903EP	2017-09-03	03:30:01.788	41.2982	129.0742	0.76	Nuclear Test
20170903CL	2017-09-03	03:38:32.553	41.3014	129.0710	0.69±0.53	Onsite Collapse
20170923EQ1	2017-09-23	04:42:59.210	41.3729	129.0468	5.8 ±2.9	Earthquake
20170923EQ2	2017-09-23	08:29:17.714	41.3708	129.0480	5.6±2.7	Earthquake
20171012EQ	2017-10-12	16:41:07.583	41.3732	129.0482	5.8 ±2.8	Earthquake

2. High-precision Relative Locations

We determine the high-precision relative locations of these small events using the relative arrival times of Pg, Pb, Pn, PnPn, sPnPn and Sn between the events (Fig. 2). Since these events occurred in a close proximity, using the relative arrival times of the seismic phases between the events would cancel out the effects of the seismic heterogeneities along the seismic traveling paths, and thus provide high-precision relative locations between the events. The relocation places event 20170903CL 440 m northwest (Fig. 1C) and event 20170923EQ2, 20170923EQ1 and 20171012EQ 8.4 km north (Figs. 1F, 1I, 1L) of the nuclear test 20170903EP.

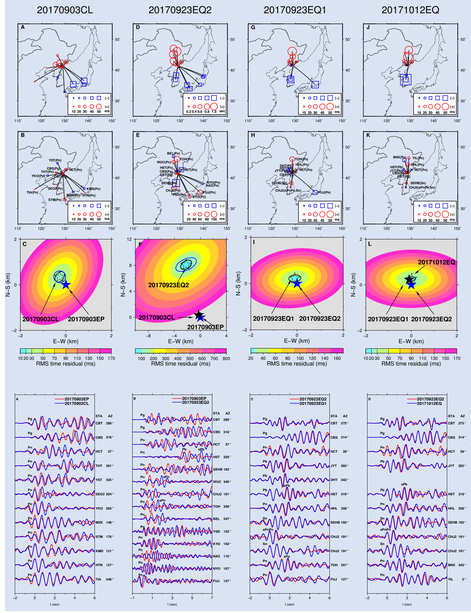

Fig. 1. Relative locations of the five events in this study. (A-C) 20170903CL relative to 20170903EP: **(A)** Relative arrival time residuals (circles and squares) of seismic phases between the two events before relocation, plotted at the locations of each station. **(B)** Relative travel time residuals based on the best-fitting relative location between the two events. **(C)** Best-fitting location of 20170903CL (open star) relative to 20170903EP (blue star) that minimizes the root-mean-square (RMS) travel time residuals of the seismic phases between the two seismic events. The black ellipse represents the 95% confidence ellipse for the location of 20170903CL based on the chi-square distribution. The blue ellipse represents location uncertainty due to an arrival time picking error of 0.05 s. **(D-F)** 20170923EQ2 relative to 20170903EP. The blue ellipse represents location uncertainty due to an arrival time picking error of 0.2 s. **(G-I)** 20170923EQ1 relative to 20170923EQ2. **(J-L)** 20171012EQ relative to 20170923EQ2.

Fig. 2. Waveform comparisons between event pairs used in relocation. In each panel, waveforms of the reference event (red traces) are aligned along the handpicked arrival times, while those of the relocated event (blue traces) are aligned according to the predicted arrival times based on the best-fitting relative location and origin time between the event pair.
(A) event pair 20170903CL and 20170903EP
(B) event pair 20170923EQ2 and 20170903EP
(C) event pair 20170923EQ1 and 20170923EQ2
(D) event pair 2017102EQ and 20170923EQ2

3. Mechanism of the onsite collapse

We study source mechanism of event 20170903CL based on various seismic observations:

- polarities of compressional body waves (Pg, Pn, Pb, PnPn and tele seismic P) (Figs. 3C, 4A)
- polarities of surface Rayleigh waves (Figs. 3D, 4B)
- differential travel times of Rayleigh waves between 20170903CL and 20170903EP (Fig. 3E)
- amplitude ratios between surface Love and Rayleigh waves (Fig. 3F)
- waveforms of Rayleigh and Love waves (Fig. 6).

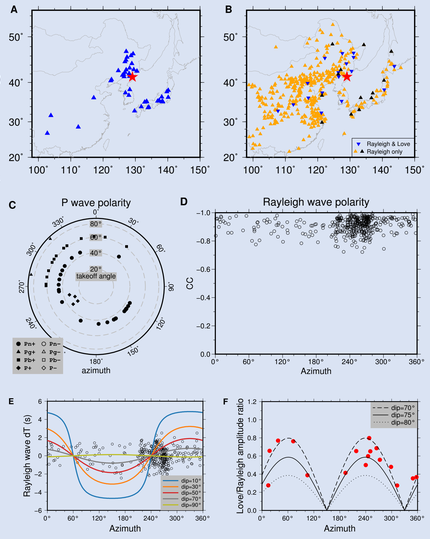

Fig. 3. Seismic data of event 20170903CL and predictions of some example single forces. (A-B) Locations of event 20170903CL and the nuclear test event 20170903EP (red star) and seismic stations (triangles) that recorded **(A)** high-quality body waves and **(B)** high-quality Rayleigh waves (triangles) and Love waves (blue inversed triangles) for both events. **(C)** Observed P wave (Pn, Pg, Pb and teleseismic P) polarities (solid symbols represent positive polarities and open symbols negative polarities) of 20170903CL relative to those of 20170903EP, shown on a focal sphere. **(D)** Relative polarities of Rayleigh waves between 20170903CL and 20170903EP as a function of azimuth, represented by Rayleigh waveform cross-correlation coefficients of the two events (negative values mean flipped polarities). **(E)** Differential travel times of Rayleigh waves (open circles) between 20170903CL and 20170903EP as a function of azimuth, along with the predicted Rayleigh wave time shifts with respect to an explosive source (colored curves) for single forces with an azimuth of 150° and various dip angles. Predictions are corrected for the effects of location difference (Fig. 1C) between 20170903CL and 20170903EP. **(F)** Observed Love/Rayleigh wave amplitude ratios of 20170903CL, along with the predictions for single forces with an azimuth of 150° and dip angles of 70° (dashed curve), 75° (solid curve) and 80° (dotted curve). Synthetic fitting of the observed Rayleigh and Love waveforms are presented in Fig. 6.

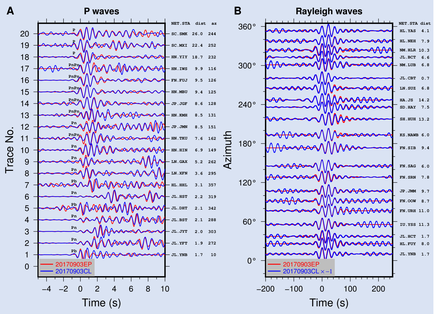

Fig. 4 Comparisons of observed waveforms of P wave and Rayleigh wave between event 20170903CL and the nuclear test event 20170903EP. (A) Waveform comparisons of P waves between 20170903CL (blue traces) and 20170903EP (red traces). Waveforms of 20170903EP are aligned by the handpicked arrival times, whereas waveforms for 20170903CL are aligned according to the travel times predicted based on the best-fitting relative location and origin time between the two seismic events. **(B)** Example Rayleigh waveform comparisons between 20170903CL (blue traces) and 20170903EP (red traces) for some example stations.

Event 20170903CL produced same first motion for all P waves recorded (Figs. 3C, 4A) and a completely reversed Rayleigh waveforms with respect to those of the nuclear test 20170903EP (Figs. 3D, 4B). This information excludes the possibility of event 20170903CL being another explosion or an implosion. The observed polarities would further exclude a double-couple earthquake source as its mechanism. We search all possible double-couple source parameters and check the percentage of the observed polarities a potential double couple source can explain and the consistency of the predicted Love/Rayleigh wave amplitude ratio of a double couple force with the observations. While there is a range of the double-couple sources can explain the Rayleigh wave polarities across the azimuths, no double-couple source can explain all the observed body wave polarities (Figs. 5A, 5B).

All 20170903CL seismic observations can be consistently explained by **a near vertical single force** and the observations place good constraints on the azimuth and dip angle of the force. The observed Love/Rayleigh ratios further narrow the **dip angle of the force to be between 70° and 75°**, with an **azimuth of about 150°** (Fig. 3F). Such a single force also predicts synthetic waveforms of Rayleigh wave and Love wave that match the observations well across all azimuths (Fig. 6).

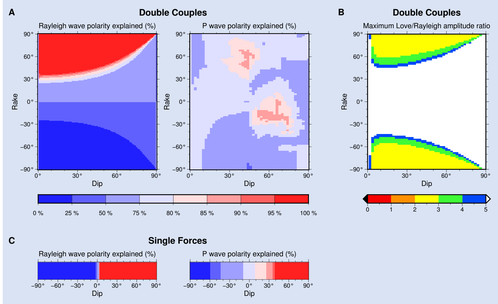

Fig. 5 Percentage of Rayleigh wave and P wave polarities explained by double couple forces and single forces (A, C), as well as predicted Love/Rayleigh ratios for double couple forces (B). (A) Percentage of Rayleigh wave polarities (left) and P wave polarities (right) explained for all possible double couple forces represented by earthquake fault parameters of rake, dip and strike. For each combination of rake and dip angles, the value of polarities explained represents the maximum value across all possible strike directions. **(B)** Maximum Love/Rayleigh amplitude ratios predicted for all possible double couple forces at all azimuths. The area in white indicates the focal mechanism parameters that would predict a maximum value of Love/Rayleigh ratios greater than 5. **(C)** Same as A, except for all possible single forces represented by the azimuth and dip angle. For each dip angle, the value of polarities explained represents the maximum value across all possible azimuths of the force.

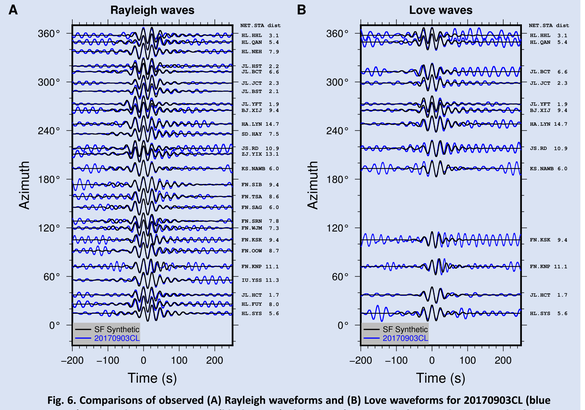

Fig. 6. Comparisons of observed (A) Rayleigh waveforms and (B) Love waveforms for 20170903CL (blue traces) and synthetic seismograms (black traces) of the best-fitting single force with an azimuth of 150° and a dip angle of 72°. Waveforms are plotted as a function of azimuth with seismic network initial, station name and epicentral distance indicated at the right of each waveform pair. Synthetics are calculated based on IASP91 model by a reflectivity method. Both observed waveforms and synthetic seismograms are bandpass filtered in the period of 20-33 s.

4. Focal Mechanism & Depth of Earthquake Swarm

Event 20170923EQ2 is a naturally earthquake, with a focal depth of at least 2.9 km (Fig. 8). We study the focal mechanism of event 20170923EQ2 based on the observed P wave polarities of the event (Fig. 7), which can be explained by nearly pure strike-slip with high dip angles of 50°-90° and strike along south-north directions. Events 20170923EQ1 and 20171012EQ exhibit almost identical waveforms to 20170923EQ2, indicating that those earthquakes are an earthquake swarm occurring in similar locations with similar focal mechanisms.

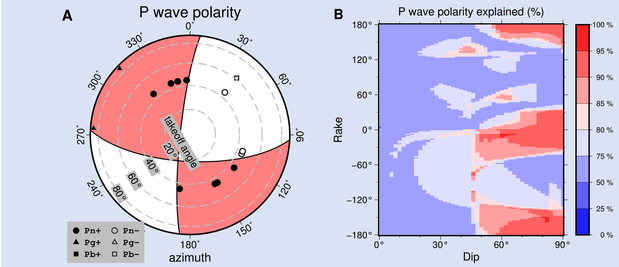

Fig. 7. Best-fitting focal mechanism of event 20170923EQ2 based on P wave polarities. (A) Observed P wave (Pn, Pg and Pb) polarities of 20170923EQ2 relative to those of the nuclear test 20170903EP. The solid and open symbols represent positive and negative polarities, respectively. The two up-going Pg observations (triangles) are plotted on the lower-hemisphere of the best-fitting focal mechanism for a better display. **(B)** Percentage of P wave polarities explained, for all possible double couple solutions. For each combination of rake and dip angles, the value of P wave polarities explained represents the maximum value across all possible strike directions.

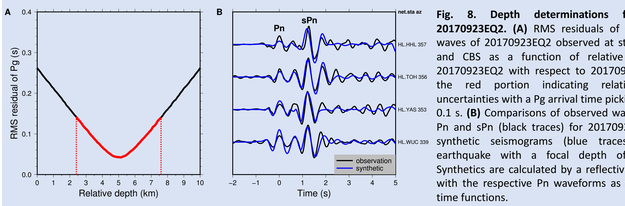

Fig. 8. Depth determinations for event 20170923EQ2. (A) RMS residuals of seismic Pg waves of 20170923EQ2 observed at stations CBT and CBS as a function of relative depth of 20170923EQ2 with respect to 20170903EP, with the red portion indicating relative depth uncertainties with a Pg arrival time picking error of 0.1 s. **(B)** Comparisons of observed waveforms of Pn and sPn (black traces) for 20170923EQ2 and synthetic seismograms (blue traces) for an earthquake with a focal depth of 3.1 km. Synthetics are calculated by a reflectivity method with the respective Pn waveforms as the source time functions.

5. Conclusion

The North Korea's 3 September 2017 nuclear test has resulted in an on-site collapse toward the nuclear test point and triggered an earthquake swarm about 8.4 km north of the test site. The occurrence of the collapse should deem the underground infrastructure beneath mountain Mantap not be used for any future nuclear tests. The triggered earthquake swarm indicates that North Korea's past tests have altered the tectonic stress in the region to the extent that previously inactive tectonic faults in the region have reached their state of critical failure.

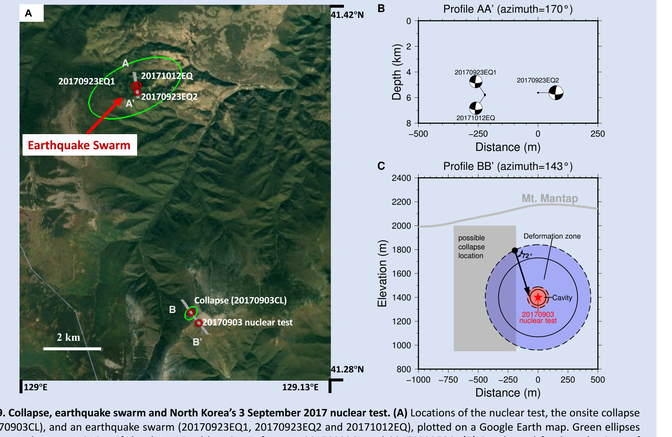

Fig. 9. Collapse, earthquake swarm and North Korea's 3 September 2017 nuclear test. (A) Locations of the nuclear test, the onsite collapse (20170903CL), and an earthquake swarm (20170923EQ1, 20170923EQ2 and 20171012EQ), plotted on a Google Earth map. Green ellipses represent the uncertainties of the determined locations of events 20170903CL and 20170923EQ2. **(B)** Depths and focal mechanisms of earthquake swarm along profile AA'. **(C)** A cross section along profile BB', showing possible zone of collapse location determined by seismic data (gray shaded region), center of the nuclear explosion (red star), and estimated cavity (light red region) and zone of elastic deformation (light blue region) associated with the nuclear test. Solid and dashed circles represent estimated cavity and zone of elastic deformation based on a nuclear test yield of 105 kt and 250 kt respectively. Arrow indicates an inferred scenario of the collapse.